A Letters Journal Exploring the Frontiers of Physics

April 2012

EPL, **98** (2012) 16002
doi: 10.1209/0295-5075/98/16002

www.epljournal.org

Suppression of atomic friction under cryogenic conditions: The role of athermal instability in AFM measurements

Y. Dong[1(a)], H. Gao[2] and A. Martini[2(b)]

[1] *School of Mechanical Engineering, Purdue University - West Lafayette, IN 47907, USA*
[2] *School of Engineering, University of California Merced - Merced, CA 95343, USA*

received 9 February 2012; accepted in final form 8 March 2012
published online 21 March 2012

PACS 68.35.Af – Atomic scale friction
PACS 07.79.Lh – Atomic force microscopes

Abstract – A theoretical investigation of the behavior of atomic friction at low temperatures is performed using a master equation method with a two-mass, two-spring Prandtl-Tomlinson model of an atomic force microscope experiment. A novel approach is taken in which two distinct instability mechanisms are introduced into the model: thermal activation is described by transition state theory with a prefactor associated with the frequency of the tip apex, and athermal instability is introduced by an Arrhenius-like equation with a prefactor associated with the characteristic frequency of the cantilever. Thermal instability causes the often reported decrease of friction with temperature followed by a stable low-friction region at high temperatures. However, the introduction of the athermal term that describes other instability mechanisms extends the predictive capability of the model such that it captures the friction plateau observed at very low temperatures.

Introduction. – Single-asperity friction, usually at the scale of nanometers, is considered the basic element of friction on all length scales and has been intensively investigated in recent years [1,2]. Atomic force microscopy (AFM) is the primary experimental tool used to study this phenomenon [3]. In a typical AFM friction measurement, the AFM cantilever drags a nanoscale sharp tip (representing a single asperity) to slide against a substrate. The resulting interaction is recorded by measuring the deformation of the cantilever. This measurement reflects the movement of the AFM tip over the substrate and the associated friction force. Although the cantilever support moves at a constant speed, the tip typically moves over the substrate in an unsteady pattern that exhibits rapid periods of motion (slip) separated by relatively longer quasi-static periods (stick). When these patterns are regular, the friction force exhibits a saw-tooth pattern that is referred to as stick-slip friction. Regardless of the regularity of the movement, the transition from stick to slip is critical to the overall frictional behavior of the system. This transition occurs when the energetic components of the system enabling motion (elastic energy in the cantilever and other instabilities) are greater than the energetic components of the system resisting motion (interaction force between tip and substrate). Characterizing these energetic contributions and their role in atomic friction is a critical step towards understanding sliding phenomena.

One of the key sources of instability believed to dominate slip motion at the atomic scale is thermal energy. This process, called thermal activation, occurs when temperature provides the system with enough additional energy to slip before the stored elastic energy overcomes the energy barrier resisting motion. Thermal activation was introduced to the atomic friction community from the theoretical perspective by Gnecco *et al.* [4] and Sang *et al.* [5]. Their widely used model predicts that a direct result of thermal activation is a monotonic decrease of friction with increasing temperature. This behavior has since been verified directly or indirectly through molecular-dynamics simulation and AFM experiments [6–10]. Recent advancements in AFM technology have allowed measurements to be taken over a wider range of temperatures, including very low (cryogenic) temperature regimes. Such measurements provide new opportunities to understand the mechanisms underlying atomic friction. The emerging experimental methods have revealed a variety of new trends. For example, distinct friction behaviors were

(a) E-mail: dong5@purdue.edu
(b) E-mail: amartini@ucmerced.edu

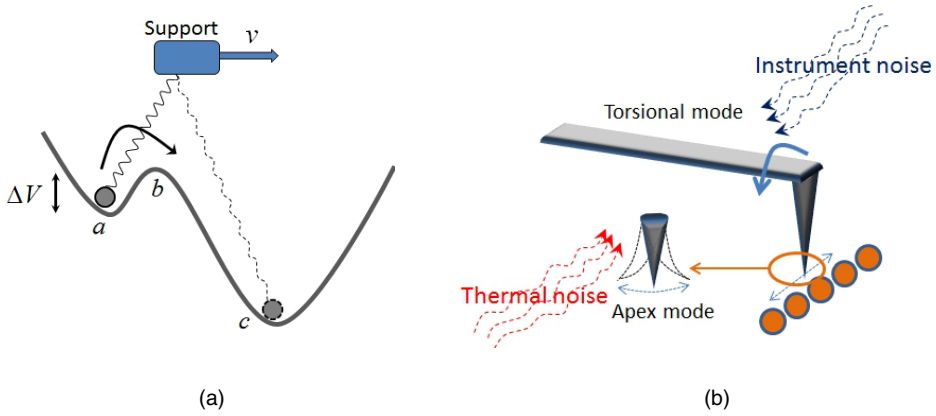

Fig. 1: (Colour on-line) (a) Support moving at constant velocity v over the energy landscape created by an atomically flat surface illustrating the energy barrier ΔV, the local potential minima a and c, and the saddle point b. (b) Schematic illustration of instability sources in an AFM system. The AFM instrument noise comes into play through the cantilever and is associated with the cantilever vibration mode, while thermal activation is localized at the tip apex region and thus associated with the tip apex mode.

observed across the superconduction phase transition of Nb films which were attributed to the suppression of electronic friction [11]. Friction measurements over wide temperature ranges on silicon, SiC wafers, ionic crystals, and graphite exhibited a friction peak around 50–200 K that was argued to be due to competition between formation of multiple bonds and thermal activation [12–14]. In a recent work, AFM measurements of an Si_3N_4 probe tip sliding against the basal plane of an a MoS_2 substrate revealed a friction plateau under cryogenic conditions [15]. Clearly thermal activation alone cannot interpret all of these very different experiment results and there is a need for theoretical support to help explain the new discoveries.

Although thermal activation may be the dominant player at most temperatures, it is not the only mechanism. Despite efforts to suppress noise levels in AFM measurements, due to the extreme sensitivity of the nanoscale contact between the tip and substrate, any instability source could play a significant role in atomic friction [16,17]. Instability sources such as mechanical vibration, acoustic noise and electromagnetic interference are inherent in the AFM instrumentation but have long been neglected in theoretical studies. In this work, we introduce instrument noise into a theoretical model and investigate its potential impact on AFM measurements of atomic friction, especially under low temperatures where thermal noise is at a minimum.

Modeling AFM measurement of atomic friction. – The master equation is a general concept in statistical mechanics and has been widely used to describe systems where a set of states exists and the occupation of these states is governed by the dynamics of transitions between them [18]. Atomic friction, which is characterized by stick and slip, falls into this rate process category, and this approach has recently been applied to study the role of thermal activation [19,20]. The master equation approach benefits from the fact that it requires fewer assumptions than other commonly used methods and so it is expected to give more accurate results.

The physical scenario of atomic friction is well described by the Prandtl-Tomlinson (PT) model [21,22]. In a typical PT model, a single asperity is modeled as a ball-like tip dragged to slide against a rigid substrate by a support displaced at constant velocity through a harmonic spring. A good assumption is that there is a single available potential energy well downward (in the direction of the support displacement); in other words, only single stick-slip occurs. This assumption holds true most of the time experimentally [2]. As shown in fig. 1(a), the tip resides at the local minima a and there is an energy barrier ΔV that hinders slipping to the next potential well c. Due to instability which may stem from thermal activation or arise from the AFM instrument noise [23], the tip is capable of sliding to the next energy well, *i.e.* slip from a to c, before the energy barrier disappears. The relationship between the thermal and athermal instabilities and an AFM contact is illustrated in fig. 1(b).

The probability of the tip occupying the available states can be described by the master equation,

$$\begin{aligned} \frac{\mathrm{d}P_a}{\mathrm{d}t} &= \kappa_{c\to a}P_c - \kappa_{a\to c}P_a, \\ \frac{\mathrm{d}P_c}{\mathrm{d}t} &= \kappa_{a\to c}P_a - \kappa_{c\to a}P_c, \end{aligned} \tag{1}$$

where $\kappa_{a\to c}$ is the instantaneous transition rate from state a to state c. Once the time-dependent probability of occupying each state (P_a and P_c) is determined, physical qualities can be obtained as weighted average over the different states. For example, the instantaneous friction $F(t)$ can be formulated as

$$F(t) = P_aF_a + P_cF_c, \tag{2}$$

where S is the displacement of the support, $F_a = k[S - x_a]$ is the friction force at state a, and similarly F_c is the friction force at state c. Using this we can obtain the average friction corresponding to different velocities and temperatures.

A numerical solution for the master equation requires information about the transition rates between available states. The transition rate stemming from thermal activation can be well described by the Arrhenrius equation,

$$\kappa_h = f_h \exp\left[-\frac{\Delta V}{k_B T}\right], \tag{3}$$

where f_h is the prefactor (or attempt frequency), ΔV is the energy barrier as shown in fig. 1(a), k_B is the Boltzmann constant and T is temperature. Based on harmonic transition state theory (HTST) [24] the prefactor for a transition from local minimum a over saddle b can be calculated through

$$f_h = \frac{1}{2\pi}\frac{\prod_{i=1}^{N}\lambda_i^{(a)}}{\prod_{j=1}^{N-1}\lambda_j^{(b)}}, \tag{4}$$

where $\lambda_i^{2(a)}$ and $\lambda_j^{2(b)}$ are the real vibrational eigenfrequencies at the minimum a and saddle point b, respectively. Note that the transition rate calculated based on HTST neglects the effect of damping. Although damping can be introduced into the analysis using Kramer's theory [24], its role in atomic friction (under-damped or over-damped) is still controversial [25,26]. Therefore, we use HTST which gives the upper limit of a realistic prefactor.

Instability sources other than those associated with thermal activation are transmitted to the tip/substrate interaction through the cantilever and can be characterized by a white noise. This white noise source will lead to a transition rate that follows an Arrhenius-like law [24],

$$\kappa_a = f_a \exp[-\beta_a \Delta V], \tag{5}$$

where f_a is the athermal attempt frequency, and β_a is the parameter characterizing the strength of the white noise. β_a can be thought of as being analogous to $k_B T$ in thermal activation, but in the case of instrument noise, it is independent of temperature. We can further assume that thermal activation and athermal instability are uncorrelated and thus independent of each other. So the transition rates originating from the two instabilities sources can be summed to give the transition rate of the whole system, $\kappa = \kappa_h + \kappa_a$.

Localized thermal activation. – Before applying this method to analyze the effects of thermal and instrument noise, we have to determine the order of magnitude of the two prefactors, f_h and f_a. The instrument noise is generated in AFM through the process of controlling the micro cantilever's displacement vertically or laterally, and then transmitted to the nano contact between tip and substrate through the cantilever. Therefore, the attempt frequency for the instrument noise can be assumed to be on the order of the characteristic frequency of the cantilever (torsional or vertical). A typical value for this frequency in a commercial AFM is $f_a = 50\,\mathrm{kHz}$ [2,27].

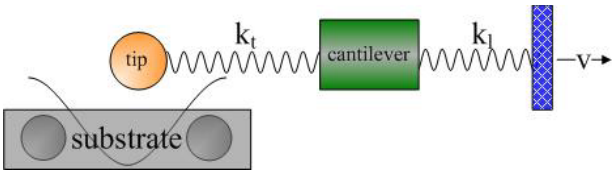

Fig. 2: (Colour on-line) Illustration of a two-spring, two-mass Prandtl-Tomlinson model. The support moving at a constant velocity drags the cantilever and the tip along the substrate. k_t and k_l are the tip and cantilever stiffness, respectively.

The attempt frequency for thermal activation is less straightforward to define. It has been argued that the flexibility of the tip apex (as opposed to the cantilever and body of the tip) plays a dominant role in thermal activation and, as a result, the effective mass is only a cluster of atoms which corresponds to an attempt frequency on the order of GHz [28–30]. We can theoretically evaluate this assumption and characterize the prefactor using transition state theory with a two-spring, two-mass PT model [28,30–33].

Figure 2 illustrates a representative setup for the two-spring, two-mass model in which the support (the rightmost part) moves at a constant velocity to drag the cantilever with a mass m_l and the tip apex with a mass m_t to slide against the substrate. Two springs k_t and k_l are used to simulate the interaction between the tip and cantilever, and between the cantilever and the support, respectively. The interaction between the tip and the substrate is modeled by a corrugation potential with a sinusoidal form which assumes that the substrate is rigid and no wear occurs during sliding.

The total energy of the system $V(x_t, x_l, t)$ is formulated as

$$V(x_t, x_l, t) = -\frac{U}{2}\cos\left(\frac{2\pi x_t}{a}\right) + \frac{1}{2}k_t(x_l - x_t)^2 + \frac{1}{2}k_l(vt - x_l)^2, \tag{6}$$

where U is the amplitude of the sinusoidal corrugation potential, x_t is the displacement of the tip apex, x_l is the displacement of the cantilever, t is the time, and v is the sliding speed of the support. We use a lattice spacing $a = 2.88\,\text{Å}$, and corrugation potential amplitude $U = 1.5\,\mathrm{eV}$. These parameters are consistent with those commonly reported for the PT model and are believed to have general implications [34]. The cantilever mass m_l varies with cantilever size and shape [27], and a typical value of $1 \times 10^{-12}\,\mathrm{kg}$ [5] is used here. The tip apex is comprised of tens to thousands of layers of atoms, which suggests that its effective mass is on the order of $m_t = 10^{-20}\,\mathrm{kg}$ [28–30].

An estimation of the tip apex stiffness k_t can be obtained indirectly. The effective stiffness k_{eff} is the

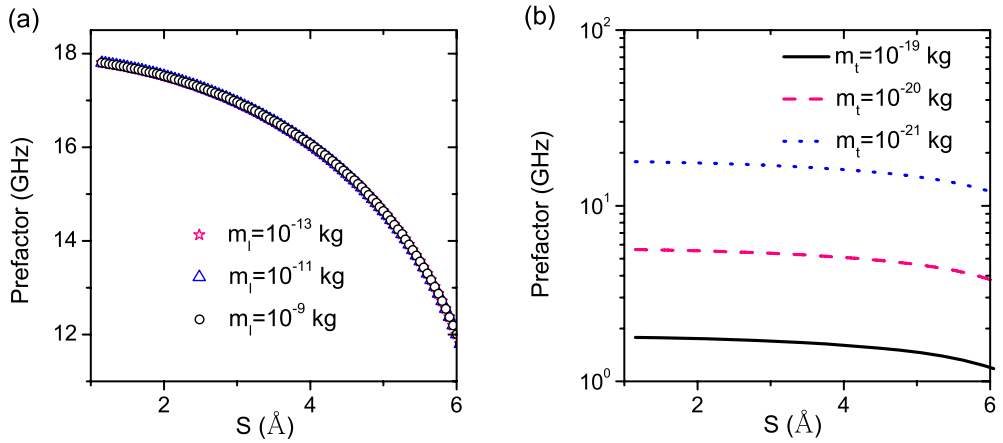

Fig. 3: (Colour on-line) Prefactor as a function of support displacement S demonstrating the effect of cantilever (a) and tip apex (b) masses. In (a) the tip apex mass is fixed at $m_t = 10^{-21}$ kg, and in (b) the cantilever mass is fixed at $m_l = 10^{-12}$ kg.

combination of the three stiffness components,

$$\frac{1}{k_{eff}} = \frac{1}{k_l} + \frac{1}{k_t} + \frac{1}{k_{cont}}, \tag{7}$$

where k_{cont} is the stiffness of the contact area. The magnitude of k_{eff} can be obtained from the gradient of a friction *vs.* the displacement curve. The effective stiffness in the context of atomic friction has been reported to be in the order of 1 N/m from experiments on different materials [6,35]. The cantilever stiffness k_l can be measured directly and is usually not less than 5 N/m [36,37]; here we take a value of $k_l = 10\,\mathrm{N/m}$. Finally, the contact stiffness k_{cont} can be roughly calculated by $\frac{2\pi^2 U}{a^2}$ which is also much larger than 1 N/m [6]. This leads to the conclusion that the flexibility of the tip apex is on the order of 1 N/m [31].

We next calculate the prefactor in eq. (3) using the well-known harmonic transition rate theory [24]. At a fixed S, the local minima and the transition point can be calculated by

$$\frac{\partial V(S, x_t, x_l)}{\partial x_t} = 0, \tag{8}$$

$$\frac{\partial V(S, x_t, x_l)}{\partial x_l} = 0. \tag{9}$$

We then perform a normal-mode analysis of the full Hamiltonian at the saddle point and the local minima. Based on the harmonic approximation, the normal modes can be derived through constructing a Hessian matrix. To obtain the Hessian matrix, we first transform eq. (6) in terms of mass-weighted coordinates $q_i = x_i\sqrt{m_i}$,

$$V(S, q_l, q_t) = -\frac{U}{2}\cos\left(\frac{2\pi q_t}{a\sqrt{m_t}}\right) + \frac{1}{2}k_t\left(\frac{q_t}{\sqrt{m_t}} - \frac{q_l}{\sqrt{m_l}}\right)^2 + \frac{1}{2}k_l\left(S - \frac{q_l}{\sqrt{m_l}}\right)^2. \tag{10}$$

The elements of the Hessian matrix can be derived by $H_{ij} = \frac{\partial^2 V}{\partial q_i \partial q_j}$. For the two-spring, two-mass model, the Hessian matrix is

$$\begin{pmatrix} \frac{k_l + k_t}{m_l} & -\frac{k_t}{\sqrt{m_t m_l}} \\ -\frac{k_t}{\sqrt{m_l m_t}} & \frac{2\pi^2 U}{a^2 m_t}\cos\left(\frac{2\pi q_t}{a\sqrt{m_t}}\right) + \frac{k_t}{m_t} \end{pmatrix}. \tag{11}$$

With the Hessian matrix, we can obtain the eigenvalues at local minima x_a and saddle point x_b and therefore deduce the prefactor.

Equipped with this method to calculate the prefactor, we can evaluate the effect of the cantilever mass and tip apex mass separately. Figures 3(a) and (b) show how the prefactor evolves with support displacement. In fig. 3(a) the mass of the cantilever is varied over four orders of magnitude with no noticeable effect on the prefactor. However, when the mass of the tip apex is varied in fig. 3(b), the prefactor changes correspondingly. This analysis shows that the prefactor for thermal activation f_h is determined by the tip apex instead of the cantilever; the effect of this localization is that its magnitude is on the order of GHz. Since the prefactor directly affects the transition rate κ_h, this theoretical analysis supports the previous suggestion [28–30] that it is the tip apex and its flexibility, instead of the whole cantilever, which directly affect thermal activation.

Athermal instability and friction plateau under cryogenical conditions. – Having estimated the magnitudes of the prefactors for the thermal and athermal instability mechanisms, we can calculate the corresponding transition rates, κ_h and κ_a, and analyze their effect on the temperature dependence of friction. Based on the analysis in the previous section, we use $f_h = 5\,\mathrm{GHz}$ and $f_a = 50\,\mathrm{kHz}$. The only remaining parameter is the instrumental noise level β_a. As an estimate we assign a value of $\beta_a = k_B T_a$, where $T_a = 500\,\mathrm{K}$, although this temperature does not imply any physical meaning.

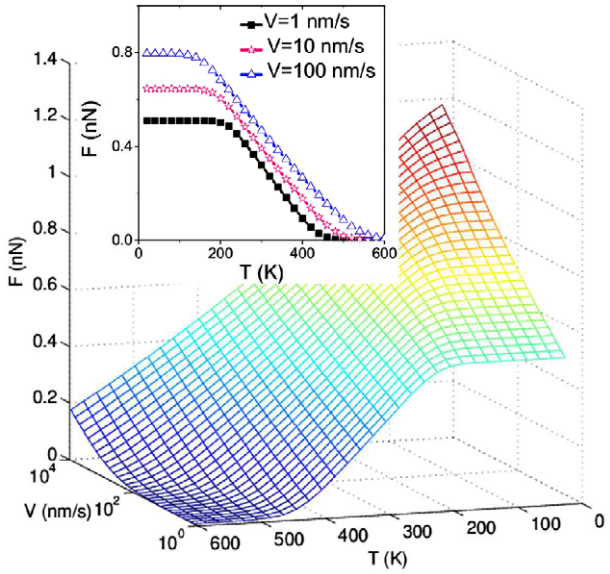

Fig. 4: (Colour on-line) Variation of the average friction with velocity and temperature with consideration of both thermal and instrument noise. The inset depicts the average friction as a function of temperature at different velocities.

Figure 4 demonstrates the variation of the average friction with velocity and temperature. As predicted by previous models, the friction approaches a constant low value at high temperatures exhibiting a behavior called thermolubrication that can be attributed to a thermally enhanced transition rate [29,30]. With the introduction of athermal instabilities, we also see a friction plateau appear at low temperatures. The formation of this plateau is due to the fact that athermal instability, which is independent of temperature, dominates at cryogenic conditions. The friction plateau that we predict at low temperature is consistent with that observed in AFM measurements performed from 100 to 500 K with an MoS_2 substrate [15].

Another interesting observation is that the transition from the low-temperature plateau to a rapid decrease of friction shifts to lower temperatures with increasing driving velocity as shown in the inset of fig. 4. Although not the focus of this paper, we also observe that the predicted velocity dependence of friction is affected by athermal instability. As shown in fig. 4, friction increases monotonically with velocity, but the rate of this increase (gradient of the $F(v)$ curve) varies with temperature. The role of athermal instability is most significant at low temperatures where, contrary to predictions of thermal activation theory, friction increases with velocity across the range of temperatures.

Conclusion. – In conclusion, we have applied a master equation method to investigate the temperature dependence of friction, especially at cryogenic conditions. Two instability sources, thermal noise and instrument noise, are considered through transition rate theory. By carrying out transition rate analysis on a two-spring PT model, we reveal that thermal noise is localized in the tip apex due to its flexibility. The instrumental noise comes into effect through the cantilever and is associated with its characteristic frequency. The impact, a friction plateau at low temperatures, is predicted and ascribed to the athermal instability induced by instrument noise.

It is important to note that several mechanisms have been proposed to explain temperature-dependent friction including thermal activation of creep motion over the energy barrier [5], thermally activated propagation of dislocations [38,39], and the occurrence of interfacial wear [15]. In addition, the present model considers only energy barriers formed by the corrugation potential. In reality, the complexity of atomic friction is beyond the description of a simple model. For example, plastic deformation, interfacial wear, aging effects [40], and bond formation and rupture [13,41,42]. We do not attempt to disprove or disregard the role of any of these mechanisms. Instead, we here postulate another mechanism, athermal instability inherent in AFM, which can describe the unexpected friction plateau at cryogenic temperatures.

The theoretical results obtained in this work encourage further temperature-dependent experimental measurements to confirm the role of the proposed mechanism. Specifically, one could perform a statistical analysis of static friction forces (force required for the tip to slip) over a range of low temperatures. If thermal activation is the only instability source, the histogram of the friction distribution, especially the width of the distribution, is a reflection of the temperature [43]. As the temperature approaches zero, the histogram becomes a delta function and the width approaches zero. The width of the friction distribution as $T \to 0\,\mathrm{K}$ can be used as an indicator of athermal instability. Another approach is to measure the temperature dependence of friction at different velocities. Since athermal instability is not a material property, but a characteristic of the AFM system, the transition point from the friction plateau to the rapid decrease of friction should vary with sliding velocity as shown in the inset of fig. 4. Such measurements, although challenging since one may need a several orders of magnitude velocity range to capture the shift of the transition temperature, would be another indicator of the existence of an athermal instability mechanism. We anticipate that these experiments and others will demonstrate the importance of athermal friction in AFM measurements and will ultimately enable the identification and understanding of the various temperature-dependent mechanisms that comprise atomic-scale friction.

* * *

We thank the National Science Foundation for its support through award CMMI-1068552, and Dr Danny Perez for helpful discussions.

REFERENCES

[1] Persson B., *Sliding friction: Physical Principles and Applications*, Vol. **1** (Springer-Verlag) 2000.
[2] Szlufarska I., Chandross M. and Carpick R., *J. Phys. D*, **41** (2008) 123001.
[3] Mate C. M., McClelland G. M., Erlandsson R. and Chiang S., *Phys. Rev. Lett.*, **59** (1987) 1942.
[4] Gnecco E., Bennewitz R., Loppacher C., Bammerlin M., Meyer E. and Guntherodt H.-J., *Phys. Rev. Lett.*, **84** (2000) 1172.
[5] Sang Y., Dube M. and Grant M., *Phys. Rev. Lett.*, **87** (2001) 174301.
[6] Riedo E., Gnecco E., Bennewitz R., Meyer E. and Brune H., *Phys. Rev. Lett.*, **91** (2003) 084502.
[7] Brukman M., Gao G., Nemanich R. and Harrison J., *J. Phys. Chem. C*, **112** (2008) 9358.
[8] Jansen L., Hölscher H., Fuchs H. and Schirmeisen A., *Phys. Rev. Lett.*, **104** (2010) 256101.
[9] Li Q., Dong Y., Perez D., Martini A. and Carpick R., *Phys. Rev. Lett.*, **106** (2011) 126101.
[10] Greiner C., Felts J., Dai Z., King W. and Carpick R., *Nano Lett.*, **10** (2010) 4640.
[11] Kisiel M., Gnecco E., Gysin U., Marot L., Rast S. and Meyer E., *Nat. Mater.*, **10** (2011) 119.
[12] Schirmeisen A., Jansen L., Hölscher H. and Fuchs H., *Appl. Phys. Lett.*, **88** (2006) 123108.
[13] Barel I., Urbakh M., Jansen L. and Schirmeisen A., *Phys. Rev. Lett.*, **104** (2010) 66104.
[14] Barel I., Urbakh M., Jansen L. and Schirmeisen A., *Phys. Rev. B*, **84** (2011) 115417.
[15] Zhao X., Phillpot S., Sawyer W., Sinnott S. and Perry S., *Phys. Rev. Lett.*, **102** (2009) 186102.
[16] Giessibl F J., *Rev. Mod. Phys.*, **75** (2003) 949.
[17] Fukuma T., Kimura M., Kobayashi K., Matsushige K. and Yamada H., *Rev. Sci. Instrum.*, **76** (2005) 053704.
[18] Zwanzig R., *Nonequilibrium Statistical Mechanics* (Oxford University Press, USA) 2001.
[19] Braun O. and Peyrard M., *Phys. Rev. E*, **82** (2010) 036117.
[20] Perez D., Dong Y., Martini A. and Voter A., *Phys. Rev. B*, **81** (2010) 245415.
[21] Tomlinson G., *Philos. Mag.*, **7** (1929) 905.
[22] Prandtl L., *Z. Angew. Math. Mech.*, **8** (1928) 85.
[23] Gammaitoni L., Hänggi P., Jung P. and Marchesoni F., *Rev. Mod. Phys.*, **70** (1998) 223.
[24] Hanggi P., Talkner P. and Borkovec M., *Rev. Mod. Phys.*, **62** (1990) 251.
[25] Roth R., Glatzel T., Steiner P., Gnecco E., Baratoff A., Meyer E. and Raman A., *Tribol. Lett.*, **39** (2010) 63.
[26] Müser M., *Phys. Rev. B*, **84** (2011) 125419.
[27] Melcher J., Hu S. and Raman A., *Appl. Phys. Lett.*, **91** (2007) 053101.
[28] Krylov S., Dijksman J., Van Loo W. and Frenken J., *Phys. Rev. Lett.*, **97** (2006) 166103.
[29] Abel D., Krylov S. and Frenken J., *Phys. Rev. Lett.*, **99** (2007) 166102.
[30] Krylov S. and Frenken J., *J. Phys.: Condens. Matter*, **20** (2008) 354003.
[31] Reimann P. and Evstigneev M., *New J. Phys.*, **7** (2005) 25.
[32] Conley W., Krousgrill C. and Raman A., *Tribol. Lett.*, **29** (2008) 23.
[33] Tshiprut Z., Filippov A. and Urbakh M., *J. Phys.: Condens. Matter*, **20** (2008) 354002.
[34] Dong Y., Vadakkepatt A. and Martini A., *Tribol. Lett.*, **44** (2011) 367.
[35] Socoliuc A., Bennewitz R., Gnecco E. and Meyer E., *Phys. Rev. Lett.*, **92** (2004) 134301.
[36] Lantz M., O'shea S., Hoole A. and Welland M., *Appl. Phys. Lett.*, **70** (1997) 970.
[37] Carpick R., Ogletree D. and Salmeron M., *Appl. Phys. Lett.*, **70** (1997) 1548.
[38] Merkle A. and Marks L., *Tribol. Lett.*, **26** (2007) 73.
[39] Liao Y. and Marks L., *Tribol. Lett.*, **37** (2010) 283.
[40] Gosvami N., Feldmann M., Peguiron J., Moseler M., Schirmeisen A. and Bennewitz R., *Phys. Rev. Lett.*, **107** (2011) 144303.
[41] Li Q., Tullis T., Goldsby D. and Carpick R., *Nature*, **480** (2011) 233.
[42] Chen J., Ratera I., Park J. and Salmeron M., *Phys. Rev. Lett.*, **96** (2006) 236102.
[43] Schirmeisen A., Jansen L. and Fuchs H., *Phys. Rev. B*, **71** (2005) 245403.